Finite-Difference Time-Domain Simulations

Elyes Balti, *Student Member, IEEE*

***Abstract*—This work discusses the Finite-Difference Time-Domain (FDTD) technique to simulate an electromagnetic wave assuming one, two and three dimensions. The propagation medium is assumed to be a free space bounded by two absorbing boundaries, perfect matched layer (PML) and perfect electric conductor (PEC). The FDTD-1D is considered in free space while FDTD-2D and 3D are considered both in free space and in a free spae-medium consisting of dielectric sphere and cylinder in the center. In this case, we model the incident and the scattered electromagnetic fields reflected back from hitting the dielectric cylinder and sphere. Moreover, the simulation starts by generating an electromagnetic pulse either in the middle or at one end of the medium and this pulse can be either Gaussian or sinusoidal. For the FDTD-3D, an antenna dipole is assumed to be the source generator of the electromagnetic pulse. We also provide the analytic solutions to confirm the accuracy of the FDTD technique.**

***Index Terms*—FDTD, PEC, PML, Scattered fields.**

I. Introduction

A. A BRIEF HISTORY OF THE FDTD METHOD

The Finite-Difference Time-Domain (FDTD) method was originally proposed by Kane S.Yee in the seminal paper he published in 1966 [1]–[17]. Yee proposed a discrete solution to Maxwells equations based on central difference approximations of the spatial and temporal derivatives of the curl-equations [18]–[25]. The novelty of Yees approach was the staggering of the electric and magnetic fields in both space and time in order to obtain second-order accuracy. Yee derived a full three-dimensional formulation, and he validated the method with two-dimensional problems. Yees method went mostly un-noticed for nearly a decade.Finally,in 1975, Taflove and Brodwin applied Yees method to simulate the scattering by dielectric cylinders and biological heating, and in 1977, Holland applied it to predict the currents induced on an aircraft by an electromagnetic pulse (EMP). Holland summarized the reason for the delay of the application of Yees method:

The algorithm was first described by Yee about ten years ago. At that time, computers did not exist which could implement this scheme practically in three dimensions. This is no longer the case. It is now possible to mesh a problem space of interest into a $30 \times 30 \times 30$ *grid and have random access to the resulting 162,000 field quantities. These advances in computer technology have prompted Longmire to credit Yees algorithm as being the fastest numerical way of solving Maxwells equations.*

The growth of the FDTD method since the late 1970s can certainly be paralleled to the ongoing advances in computer technology. In fact, with todays massively parallel computers, a grid dimension of $3.000 \times 3.000 \times 3.000$, which requires nearly 1.5 terabytes of memory, is feasible. Longmires quote above summarizes another reason for its growth. The FDTD method is a fast algorithm. If N is the total number of degrees of freedom in the three-dimensional space, each time-iteration only requires $O(N)$ floating-point operations. The caveat is that the discrete mesh has to fill the full three-dimensional space. Thus, the number of degrees of freedom grows cubically with the linear dimension of the problem domain.

Another reason for the wide-spread use of the FDTD method is its simplicity. One is reminded of Chef Auguste Gusteaus signature statement in Pixars movie Ratatouille: Anyone can cook!. Similarly, one can say: Anyone can FDTD!. The FDTD method is a wonderfully simple method that can be taught at the undergraduate or early graduate level. Yet, it is capable of solving extremely sophisticated engineering problems.

The maturation of the FDTD method can be attributed to a number of pioneers who have made a host of contributions to advance Yee's base FDTD algorithm. Each innovation has played a key role in advancing the FDTD method to where it is today.

One set of key contributions revolve around the ability of the FDTD method to simulate unbounded problems. To model such problems, the discrete domain must be truncated via a reflectionless absorbing boundary.In 1981,G.Mur proposed a second-order accurate absorbing boundary condition (ABC) that helped to resolve this issue. Later, Higdon introduced a class of boundary operators that was more versatile. Betz-and Mittra extended Higdon's ABC to absorb evanescent waves. While such ABC's were widely used, the dynamic range of the FDTD method as well as the range of applications was still limited by this class of absorbing boundaries. A much more accurate absorbing boundary based on a Perfectly Matched Layer (PML) absorbing medium was proposed by J.-P. Berenger. In fact, the reflection error of the PML can be 3 or 4 orders of magnitude smaller than that offered by an ABC. The PML was also capable of truncating unbounded media that was lossy, inhomogeneous, dispersive, non-linear, or anisotropic. Further developments of Berenger's PML also rendered it capable of absorbing evanescent waves and near fields.The tradeoff of using the PML is an extension of the mesh and additional degrees of freedom in the PML region. Thus, it is more computationally intensive than a local ABC. However, in the mid 1990's, these resources were available even with commodity computers. The direct result of this innovation was that the FDTD method with PML absorbing boundaries was capable of being applied to a much broader range of problems.

One of the advantages of the FDTD solution of Maxwells equations is that arbitrary media types can inherently be modeled. The FDTD method naturally accommodates inhomogeneous and lossy media. More complex media types, such as frequency-dependent dispersive, anisotropic, bi-anisotropic, chiral, or non-linear media can also be accommodated within the FDTD method. Significant effort has been made by researchers to develop accurate and efficient algorithms to model such media within the context of the FDTD method. An excellent summary of handling complex media within the FDTD method is provided by F. L. Teixeira.

As the FDTD method has matured, the number of application areas it has impacted has diversified. Initially, the FDTD method was applied primarily to classical areas in electromagnetics, including electromagnetic scattering, electromagnetic compatibility, antennas, microwave circuits, and wave propagation. More recently, it has also been applied a diversity of other areas, including biomedical engineering, electromagnetic environmental hazards, ground penetrating radar, photonics, biophotonics, plasmonics, photovoltaics, nano-optical storage devices, and seismic detection. The FDTD method is continuing to develop and expand. Current thrust areas include highorder FDTD methods,more general gridding techniques, unconditionally stable schemes, and multiphysics applications. With these

Elyes Balti is with the Wireless Networking and Communications Group, Department of Electrical and Computer Engineering, The University of Texas at Austin, Austin, TX 78712 USA e-mail: ebalti@utexas.edu.

endeavors and many others in progress, as well as continued advances in computing.

B. LIMITATIONS OF THE FDTD METHOD

While uncovering a historical perspective of the FDTD method, the previous section presented various strengths of the FDTD method. Of course, the method is not without its weaknesses, and it is certainly necessary to underline what these are. That is,it is important to understand the limitations of the FDTD method in order to determine when the method is most appropriately applied. One weakness of the FDTD method is that it requires a full discretization of the electric and magnetic fields throughout the entire volume domain. There are many instances when the FDTD method is forced to model a significant amount of white-space, i.e., open space with no inhomogeneities. An example could be the electromagnetic scattering of a cluster of perfectly conducting spheres. The white space would be the volume inside each sphere, as well as the region in-between the spheres and the region separating the spheres and the absorbing boundary. The wider the separation between the spheres, the larger the percentage of white space. Another example is a printed circuit in a layered media where the traces being modeled constitute a very small percentage of the volume. The fact that the FDTD method is fully explicit can also be a weakness. While this can be considered a strength since a linear system of equations is not required to be solved, it can be a weakness if the time-step becomes inordinately small. The time-step is limited by the smallest geometric feature in the model. As a consequence, models with fine, electrically small geometric features can have very small time-steps. This can result in a large number of time-iterations. This poses challenges when applying the FDTD method to large problems with fine geometric features that must be modeled with high fidelity.

The FDTD method provides a broad-band simulation. As a consequence, a broad frequency response can be analyzed via a single simulation. Again, in many circumstances, this can be considered a strength. However, there are instances when only a narrow band response is desired. As a consequence, a frequency domain simulation may be more efficient. Furthermore, when modeling complex materials, if the material constants are only known over a narrow frequency band, this characterization must be approximated over a broadband within the FDTD method. This could be as simple as the loss tangent of a substrate, or the effective material properties of a metamaterial.

The FDTD method can also be challenged when the system under test has a very high Q. Consequently, the time-domain simulation may take a very long time to reach a steady state. Often, this is due to narrow band resonances that slowly decay (if at all). Thus, very long simulation times can result. For some problems, this can be mitigated by using methods such as the Generalized Pencil of Functions to either quantify the resonances, or to extrapolate the signal. In other cases, a frequency-domain simulation about the resonant frequencies may be more expedient.

The FDTD method is also restricted by orthogonal gridding.This can be overcome by the use of subcell modeling techniques as well as sub-gridding and non-uniform grid methods. However, the local fields can still lose accuracy. Also, with methods such as subcell modeling, there is a level of uncertainty as to the exact shape of the local boundary. Thus, it is important to understand the level of accuracy of the near fields that can be achieved by subcell models for the geometry at hand. Higher-order FDTD methods have not shared the success of higher-order algorithms posed using other methodologies (such as discontinuous Galerkin methods). Most higher-order FDTD methods posed to date are based on an extended stencil namely, they are based on high-order difference approximations that employ points that span multiple grid cells. This makes it difficult to model simple geometries that involve jump discontinuities in the materials. These methods are also challenged by structures with fine geometric detail.

II. YEE ALGORITHM

The FDTD algorithm as first proposed by Kane Yee in 1966 employs second-order central differences. The algorithm can be summarized as follows:

1) Replace all the derivatives in Amperes and Faradays laws with finite differences. Discretize space and time so that the electric and magnetic fields are staggered in both space and time.
2) Solve the resulting difference equations to obtain 'update equations' that express the (unknown) future fields in terms of (known) past fields.
3) Evaluate the magnetic fields one time-step into the future so they are now known (effectively they become past fields).
4) Evaluate the electric fields one time-step into the future so they are now known (effectively they become past fields).
5) Repeat the previous two steps until the fields have been obtained over the desired duration.

III. ONE-DIMENSIONAL SIMULATION

TABLE I: Electromagnetic Parameters

Symbol	QUANTITY
$\mathbf{B}$	magnetic flux density
$\mathbf{H}$	magnetic field strength
$\mathbf{D}$	electric field density
$\mathbf{E}$	electric field strength
$\epsilon_\mathbf{0}$	permittivity of free space
$\mu_\mathbf{0}$	permeability of free space
$\epsilon_\mathbf{r}$	relative permittivity
$\mu_\mathbf{r}$	relative permeability
σ	conductivity
η	intrinsic impedance
$\mathbf{c}$	speed of light

A. FDTD Formulation

Considering Maxwell's curl equations in free space as follows:

$$\frac{\partial \boldsymbol{E}}{\partial t} = \frac{1}{\epsilon_0}\nabla \times \boldsymbol{H} \tag{1}$$

$$\frac{\partial \boldsymbol{H}}{\partial t} = -\frac{1}{\mu_0}\nabla \times \boldsymbol{E} \tag{2}$$

Given that along this work one dimension is assumed, the components E_x and H_y are only considered to facilitate the calculus and the other components are set to zeros. Given that the wave propagates in z direction, the curl equations are reduced as follows:

$$\frac{\partial E_x}{\partial t} = -\frac{1}{\epsilon_0}\frac{\partial H_y}{\partial z} \tag{3}$$

$$\frac{\partial H_y}{\partial t} = -\frac{1}{\mu_0}\frac{\partial E_x}{\partial z} \tag{4}$$

To discretize these equations in time and space, we should apply the central difference method for temporal and spatial derivatives. The above aligns can be written as follows:

$$\frac{E_x^{n+\frac{1}{2}}(k) - E_x^{n-\frac{1}{2}}(k)}{\Delta t} = -\frac{1}{\epsilon_0}\frac{H_y^n\left(k+\frac{1}{2}\right) - H_y^n\left(k-\frac{1}{2}\right)}{\Delta x} \quad (5)$$

$$\frac{H_y^{n+1}\left(k+\frac{1}{2}\right) - H_y^n\left(k+\frac{1}{2}\right)}{\Delta t} = -\frac{1}{\mu_0}\frac{E_x^{n+\frac{1}{2}}(k+1) - E_x^{n+\frac{1}{2}}(k)}{\Delta x} \quad (6)$$

where Δt and Δx are the time and the space step, respectively. n and k are the number of the time and space steps, respectively. An instant t is given by $t = n\Delta t$, while a distance z is given by $z = k\Delta x$. The discretized equations can be formulated into an iterative algorithm as follows:

$$E_x^{n+\frac{1}{2}}(k) = E_x^{n-\frac{1}{2}}(k) - \frac{\Delta t}{\epsilon_0 \Delta x}\left[H_y^n\left(k+\frac{1}{2}\right) - H_y^n\left(k-\frac{1}{2}\right)\right] \quad (7)$$

$$H_y^{n+1}\left(k+\frac{1}{2}\right) = H_y^n\left(k+\frac{1}{2}\right) - \frac{\Delta t}{\mu_0 \Delta x} \times \left[E_x^{n+\frac{1}{2}}(k+1) - E_x^{n+\frac{1}{2}}(k)\right] \quad (8)$$

Note that E_x and H_y differ by a large order of magnitude because of ϵ_0 and μ_0. To fix this problem, we will roughly normalize the magnitude of the electric field so that it becomes comparable to the amplitude of the magnetic field. The new expression of the electric field can be obtained by [**?**, eq. (1.5)]:

$$\widetilde{E} = \sqrt{\frac{\epsilon_0}{\mu_0}}E \quad (9)$$

This new expression of the electric field will be used for the analytic solution in order to get a result in agreement with the FDTD method. As we mentioned earlier, the space is equally dicretized into cells of the same size. For a given cell of size Δx, the time step is given by:

$$\Delta t = \frac{\Delta x}{2c} \quad (10)$$

where c is the speed of light.

In this work, we create a Gaussian pulse in the middle and once the pulse is launched at t_0, the wave propagates in the two directions (positive and negative z directions) until it hits the boundaries, then it reflects back. Given that the boundaries are absorbing, the waves will not be reflected back. The first boundary can be modelled as follows:

$$E_x^n(0) = E_x^{n-2}(1) \quad (11)$$

The electric field can be given at the second boundary as follows:

$$E_x^n(\mathrm{KE}) = E_x^{n-2}(\mathrm{KE}-1) \quad (12)$$

where KE is the length of the propagation medium.

B. Analytic Solution

Consider a Gaussian pulse as follows:

$$f(t) = \exp(-\sigma t^2) \quad (13)$$

The electromagnetic field is assumed to propagate in both positive and negative z directions. If the time pulse is Gaussian, the spectral density of this pulse is also Gaussian. The temporal Fourier transform of the initial pulse is given by:

$$F(\omega) = \sqrt{\frac{\pi}{\sigma}}\exp\left(-\frac{\omega^2}{4\sigma}\right) \quad (14)$$

Note that the pulse in frequency domain should be multiplied by a carrier or a propagator factor e^{-ikz} to move in the positive z direction and a carrier e^{+ikz} to move in the negative z direction. To get the expression of the electric field in time and space (positive z direction), the next step is to take the inverse of the Fourier transform of the spectral pulse multiplied by the carrier as follows:

$$E^+(z,t) = \frac{1}{2\pi}\int_0^\infty F(\omega)\ e^{-ikz}e^{+i\omega t}d\omega \quad (15)$$

The electric field $E^-(z,t)$ propagating in the negative z direction can be derived by replacing the propagating factor in eq. (15) by e^{+ikz}. Finally, the total electric field in time and space is given by:

$$E(z,t) = E^+(z,t) + E^-(z,t) \quad (16)$$

A Gaussian pulse is created at the instant t_0 in the middle of the space problem taking the following form:

$$f(T) = \exp\left[-0.5\left(\frac{t_0 - T}{\text{spread}}\right)^2\right] \quad (17)$$

The Fourrier transform of the above pulse is given by:

$$F(\omega) = \text{spread}\ e^{-\frac{(\omega\text{spread})^2}{2}}e^{i\omega t_0} \quad (18)$$

The electric field in the positive z direction can be given by:

$$E^+(z,t) = \text{spread}^2\ e^{\frac{(t_0-t)^2}{2\ \text{spread}^2}}e^{-ikz} \quad (19)$$

The electric field in the negative z direction can be given by:

$$E^-(z,t) = \text{spread}^2\ e^{\frac{(t_0-t)^2}{2\ \text{spread}^2}}e^{+ikz} \quad (20)$$

Figures 1 and 2 show clearly the agreement between the FDTD and the analytic solution for different time steps and space. As we see, the wave starts from the middle and then it propagates in the two directions until the instant T = 250. At the instant T = 150, the wave moves to other positions and it is still far from the boundaries. At the instant T = 225, the wave starts hitting the two boundaries and it roughly overtakes the two ends at the instant T = 250 and then it totally vanishes from the space problem because it is absorbed by the two boundaries.

IV. Two-Dimentional Simulation

A. Free Space Medium with Absorbing Boundaries

We will start with the normalized Maxwells equations as follows:

$$\frac{\partial \widetilde{\boldsymbol{D}}}{\partial t} = \frac{1}{\sqrt{\epsilon_0\mu_0}}\nabla \times \widetilde{\boldsymbol{H}} \quad (21)$$

$$\widetilde{\boldsymbol{D}}(\omega) = \epsilon_r^*(\omega)\cdot\widetilde{\boldsymbol{E}}(\omega) \quad (22)$$

$$\frac{\partial \boldsymbol{H}}{\partial t} = -\frac{1}{\sqrt{\epsilon_0\mu_0}}\nabla \times \widetilde{\boldsymbol{E}} \quad (23)$$

For the TM mode, the above equations reduced as follows:

$$\frac{\partial D_z}{\partial t} = \frac{1}{\sqrt{\epsilon_0\mu_0}}\left(\frac{\partial H_y}{\partial x} - \frac{\partial H_x}{\partial y}\right) \quad (24)$$

$$\boldsymbol{D}(\omega) = \epsilon_r^*(\omega)\cdot\boldsymbol{E}(\omega) \quad (25)$$

$$\frac{\partial H_x}{\partial t} = -\frac{1}{\sqrt{\epsilon_0\mu_0}}\frac{\partial E_z}{\partial y} \quad (26)$$

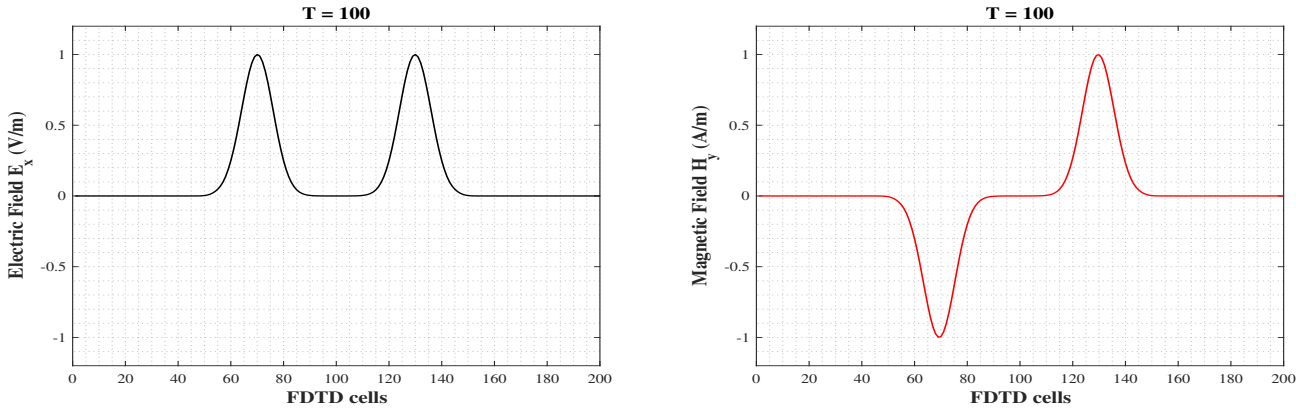

Fig. 1: FDTD-1D simulation of a Gaussian pulse in free space after 100 time steps. The pulse originated in the center and travels outward (KE = 200, t_0 = 40, spread = 12).

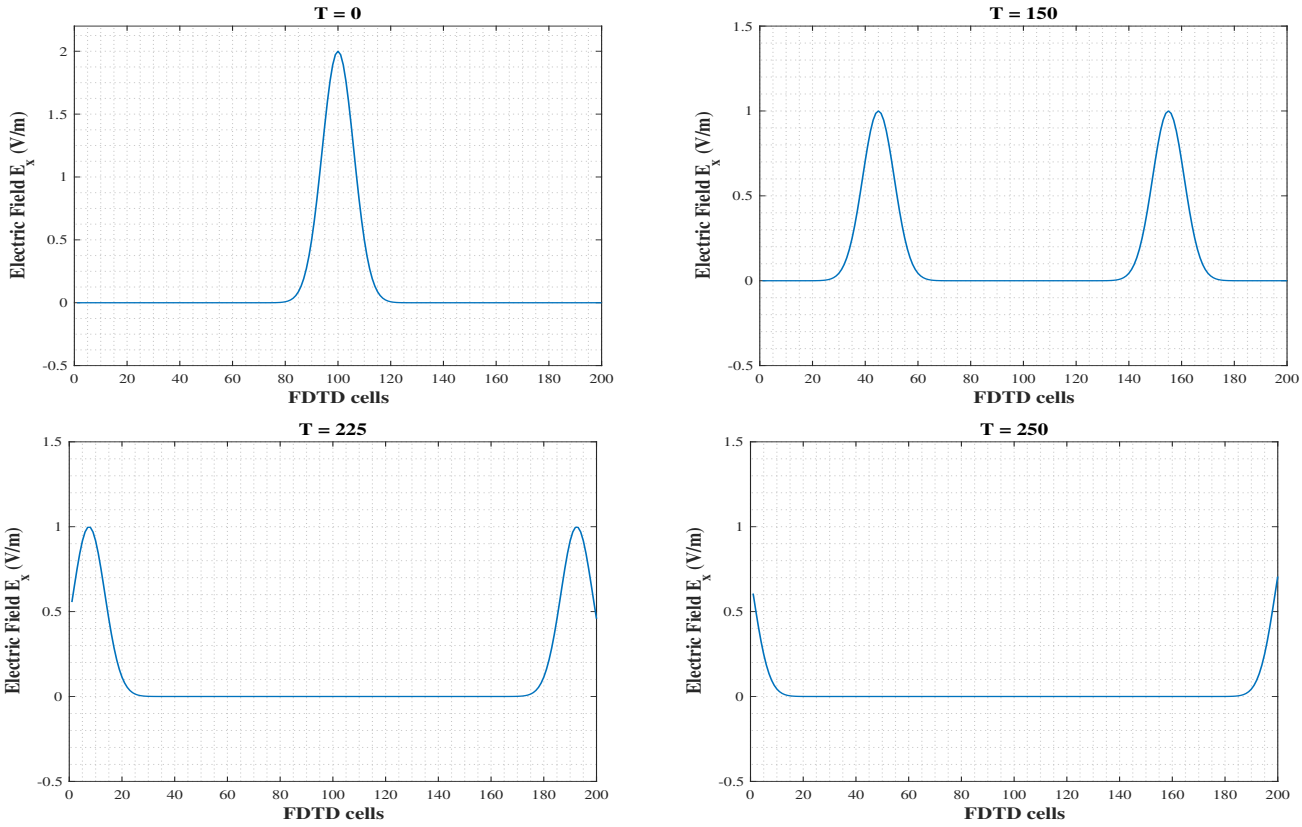

Fig. 2: Simulation of an FDTD program with absorbing boundary conditions. Notice that the pulse is absorbed at the edges without reflecting anything back.

$$\frac{\partial H_y}{\partial t} = \frac{1}{\sqrt{\epsilon_0 \mu_0}} \frac{\partial E_z}{\partial x} \tag{27}$$

The discretization of the above equations leads to:

$$\frac{D_z^{n+1/2}(i,j) - D_z^{n-1/2}(i,j)}{\Delta t} = \frac{1}{\sqrt{\epsilon_0 \mu_0}} \times \left(\frac{H_x^n\left(i+\frac{1}{2},j\right) - H_y^n\left(i-\frac{1}{2},j\right)}{\Delta x} \right) - \frac{1}{\sqrt{\epsilon_0 \mu_0}} \times \left(\frac{H_x^n\left(i,j+\frac{1}{2}\right) - H_x^n\left(i,j-\frac{1}{2}\right)}{\Delta x} \right) \tag{28}$$

$$\frac{H_x^{n+1}\left(i+\frac{1}{2},j\right) - H_x^n\left(i+\frac{1}{2},j\right)}{\Delta t} = -\frac{1}{\sqrt{\epsilon_0 \mu_0}} \times \frac{E_z^{n+1/2}(i,j+1) - E_z^{n+1/2}(i,j)}{\Delta x} \tag{29}$$

$$\frac{H_y^{n+1}\left(i+\frac{1}{2},j\right) - H_y^n\left(i+\frac{1}{2},j\right)}{\Delta t} = -\frac{1}{\sqrt{\epsilon_0 \mu_0}} \times \frac{E_z^{n+1/2}(i+1,j) - E_z^{n+1/2}(i,j)}{\Delta x} \tag{30}$$

Fig. 3 shows clearly the propagation of a Gaussian pulse generated in the middle of the space problem. We observe how the wave

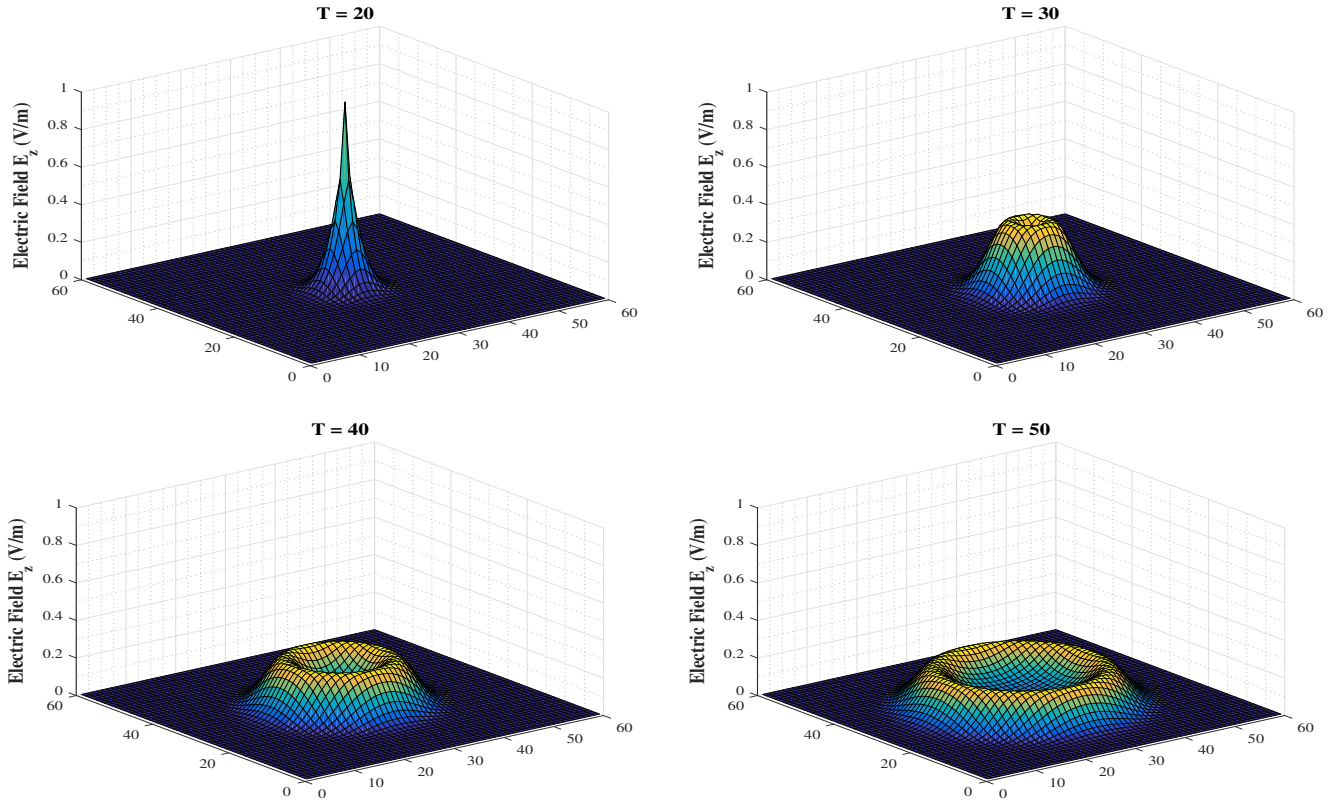

Fig. 3: FDTD-2D simulation of a Gaussian pulse in free space medium with absorbing boundaries in various time instants.

propagates in all directions till it hits the boundaries and then totally vanishes.

B. The Perfectly Matched Layer (PML)

According to Sullivan's book, the PML parameters can be presented as follows:

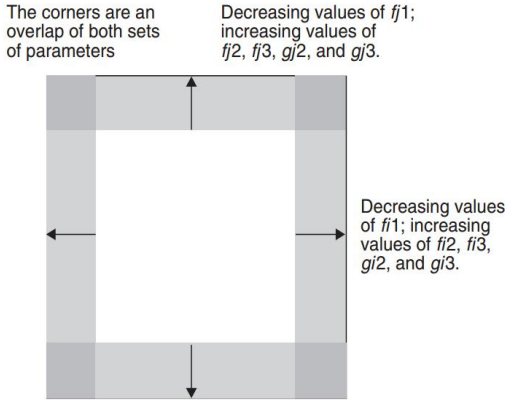

Fig. 4: Parameters related to the perfectly matched layer (PML).

Maxwell's equations can be updated as follows:

$$D_z^{n+1/2}(i,j) = gi3(i)gj3(j)D_z^{n-1/2}(i,j) + 0.5gi2(i)gj2(j) \times \left[H_y^n\left(i+\frac{1}{2},j\right) - H_y^n\left(i-\frac{1}{2},j\right) - H_y^n\left(i,j+\frac{1}{2}\right) + H_y^n\left(i,j-\frac{1}{2}\right)\right] \quad (31)$$

where $gi2, gi3, gj2, gj3$ are given by:

$$gi2 = gj2 = \frac{1}{1+\frac{\sigma\Delta t}{2\epsilon_0}}$$
$$gi3 = gj3 = \frac{1-\frac{\sigma\Delta t}{2\epsilon_0}}{1+\frac{\sigma\Delta t}{2\epsilon_0}}$$

The curl of the electric field can be given by:

$$\nabla \times \mathbf{E} = E_z^{n+1/2}(i+1,j) - E_z^{n+1/2}(i,j) \quad (32)$$

The incident magnetic field in the Y-direction can be given by:

$$I_{H_y}^{n+1/2}\left(i+\frac{1}{2},j\right) = I_{H_y}^{n-1/2}\left(i+\frac{1}{2},j\right) + \nabla \times \mathbf{E} \quad (33)$$

The total magnetic field in the Y-direction can be evaluated recursively as follows:

$$H_y^{n+1/2}\left(i+\frac{1}{2},j\right) = gi3\left(i+\frac{1}{2}\right)H_y^n\left(i+\frac{1}{2},j\right) - 0.5gi2\left(i+\frac{1}{2}\right)\nabla \times \mathbf{E} - gj1(j)I_{H_y}^{n+1/2}\left(i+\frac{1}{2},j\right) \quad (34)$$

where $gi1$ is given by:

$$gi1 = \frac{\sigma\Delta t}{2\epsilon_0}$$

The incident magnetic field in the X-direction is given by:

$$I_{H_x}^{n+1/2}\left(i,j+\frac{1}{2}\right) = I_{H_x}^{n-1/2}\left(i,j+\frac{1}{2}\right) + \nabla \times \mathbf{E} \quad (35)$$

The total magnetic field in the X-direction can be obtained by:

$$H_x^{n+1}\left(i,j+\frac{1}{2}\right) = gj3\left(j+\frac{1}{2}\right)H_x^n\left(i,j+\frac{1}{2}\right) + 0.5\ gj2\left(j+\frac{1}{2}\right)\nabla\times\mathbf{E} + gj1(j)I_{H_y}^{n+1/2}\left(i,j+\frac{1}{2}\right) \quad (36)$$

Fig. 5 shows an FDTD-2D simulation of a sinusoidal source is initiated at a point that is offset five cells from the center of the problem space in each direction. As the wave reaches the perfectly matched layer (PML), which is eight cells on every side, it is absorbed. The effectiveness of the PML is apparent in the bottom figure because the contours would not be concentric circles if the outgoing wave was partially reflected.

C. Total/Scattered Field Formulation

In order to simulate a plane wave in a two-dimensional FDTD program, the problem space will be divided into two regions, the total field and the scattered field (in below figure). The two primary reasons for doing this are (i) the propagating plane wave should not interact with the ABCs and (ii) the load on the ABCs should be minimized. These boundary conditions are not perfect, that is, a certain portion of the impinging wave is reflected back into the problem space. By subtracting the incident field, the amount of the radiating field hitting the boundary is minimized, thereby reducing the amount of error.

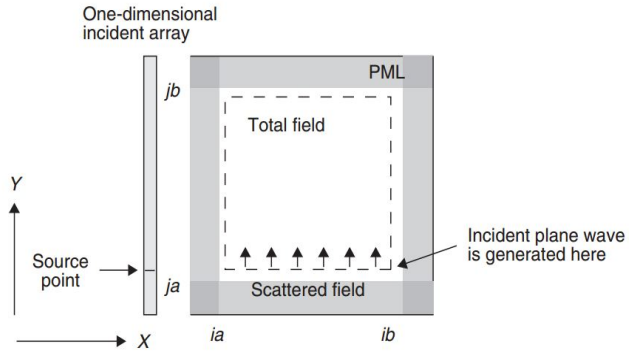

Fig. 6: Total field/scattered field of the two-dimensional space.

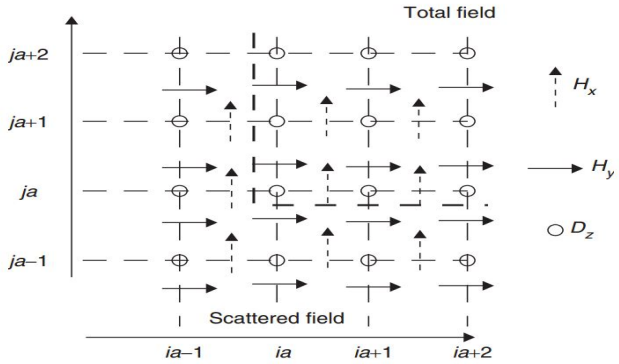

Fig. 7: Every point is in either the total field or the scattered field.

There are three places that must be modified:
The D_z value at j = ja or j = jb:

$$D_z(i,j_a) = D_z(i,j_a) + 0.5H_{x,inc}\left(j_a-\frac{1}{2}\right) \quad (37)$$

$$D_z(i,j_b) = D_z(i,j_b) - 0.5H_{x,inc}\left(j_a-\frac{1}{2}\right) \quad (38)$$

The H_x field just outside at j = ja or j = jb:

$$H_x\left(i,j_a-\frac{1}{2}\right) = H_x\left(i,j_a-\frac{1}{2}\right) + 0.5E_{z,inc}(j_a) \quad (39)$$

$$H_x\left(i,j_b+\frac{1}{2}\right) = H_x\left(i,j_b+\frac{1}{2}\right) - 0.5E_{z,inc}(j_b) \quad (40)$$

H_y just outside at i = ia and i = ib:

$$H_y\left(i_a-\frac{1}{2},j\right) = H_y\left(i_a-\frac{1}{2},j\right) - 0.5E_{z,inc}(j) \quad (41)$$

$$H_y\left(i_b-\frac{1}{2},j\right) = H_y\left(i_b-\frac{1}{2},j\right) + 0.5E_{z,inc}(j) \quad (42)$$

D. A Plane Wave Impinging on a Dielectric Cylinder

To simulate a plane wave interacting with an object, we must specify the object according to its electromagnetic propertiesthe dielectric constant and the conductivity. For instance, suppose we are simulating a plane wave striking a dielectric cylinder 20 cm in diameter, which has a dielectric constant specified by the parameter epsilon and a conductivity specified by the parameter sigma.

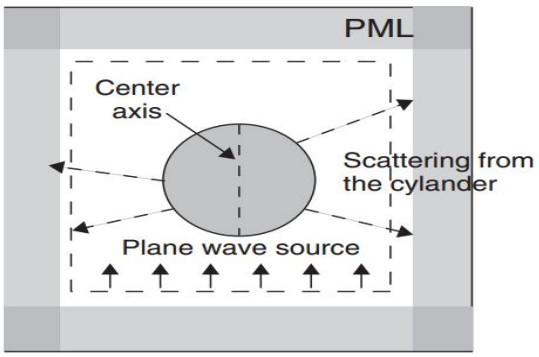

Fig. 9: Simulation of a plane wave striking a dielectric cylinder. The fields scattered from the cylinder are the only fields to leave the total field and strike the PML.

The simulation of a plane wave pulse hitting a dielectric cylinder with ϵ_r = 30 and σ = 0.3 is shown in Fig. 10. After 25 time steps, the plane wave has started from the side; after 50 time steps, the pulse is interacting with the cylinder. Some of the pulse passes through the cylinder, and some of it goes around it. After 100 steps, the main part of the propagating pulse is being subtracted from the end of the total field.

E. Analytic Solution

For the case of an electromagnetic wave propagating in free space medium bounded by PML, the propagator factor now consists of k_x and k_y (2 directions). It can be given by:

$$\text{Space Propagator} = \exp\left[-i(k_x\ x + k_y\ y)\right] \quad (43)$$

After reproducing the analysis of FDTD-1D for both X and Y directions, the analytic solution can be derived. Regarding the case of a free space medium equipped with a dielectric cylinder, the scattered field can be derived as follows:

$$E_s^{TM}(\mathbf{r}) = (E_i^0\cdot\hat{v}_i)\frac{k}{k_{i,\rho}}\sum_{m=-\infty}^{\infty}\frac{J_m(k_{i,\rho},a)}{H_m^{(2)}(k_{i,\rho}a)}(-j)^m\exp(jm\phi_i) \times N_{m,k_{i,z}}^H(\rho,\phi,z) \quad (44)$$

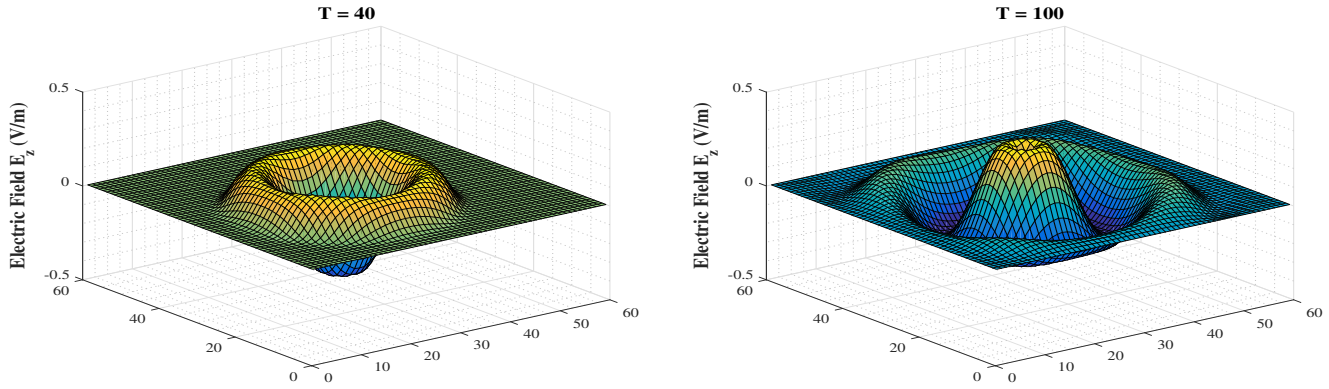

Fig. 5: FDTD-2D simulation of a sinusoidal pulse with PML in various instants.

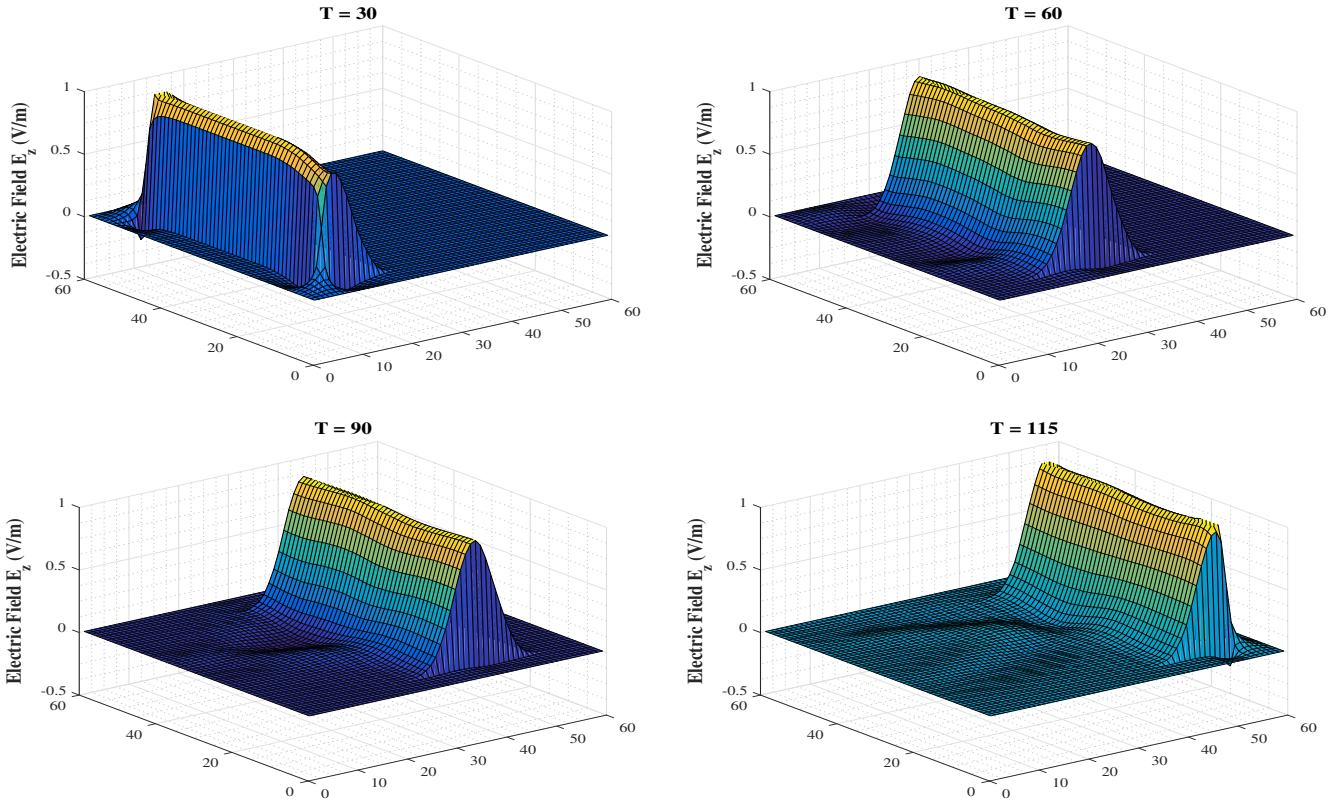

Fig. 8: Simulation of a plane wave pulse propagating in free space. The incident pulse is generated at one end and subtracted at the other end.

$$H_s^{TM}(\mathbf{r}) = -\frac{j}{\eta}\sum_{m=-\infty}^{\infty}\nu_m\frac{J_m(k_{i,\rho})}{H_m^{(2)}(k_{i,\rho})}M^H_{m,k_{i,z}}(\rho,\phi,z) \tag{45}$$

where ν_m, $M^H_{m,k_{i,z}}$, $N^H_{m,k_{i,z}}$, $\psi_{m,k_{i,z}}$ are given by:

$$\nu_m = -(E_i^0\cdot\hat{v}_i)\frac{k}{k_{i,\rho}}(-j)^m\exp(jm\phi_i)$$

$$M^H_{m,k_{i,z}} = \frac{1}{k}\nabla\times[\psi^H_{m,k_{i,z}}\mathbf{z}]$$

$$N^H_{m,k_{i,z}} = \frac{1}{k}\nabla\times[M^H_{m,k_{i,z}}]$$

$$\psi^H_{m,k_{i,z}}(\rho,\phi,z) = [AH_m^{(1)}(k_r\rho)+BH_m^{(2)}(k_r\rho)]\exp[-jm\phi-jk_zz]$$

Where $H_m^{(1)}$ and $H_m^{(2)}$ are the Hankel functions of the first and second kind, respectively.

V. Three-Dimensional Simulation

A. Free Space Simulation

Starting with Maxwell's equations, we have:

$$\frac{\partial\widetilde{\boldsymbol{D}}}{\partial t} = \frac{1}{\sqrt{\epsilon_0\mu_0}}\nabla\times\widetilde{\boldsymbol{H}} \tag{46}$$

$$\widetilde{\boldsymbol{D}}(\omega) = \epsilon_r^*(\omega)\cdot\widetilde{\boldsymbol{E}}(\omega) \tag{47}$$

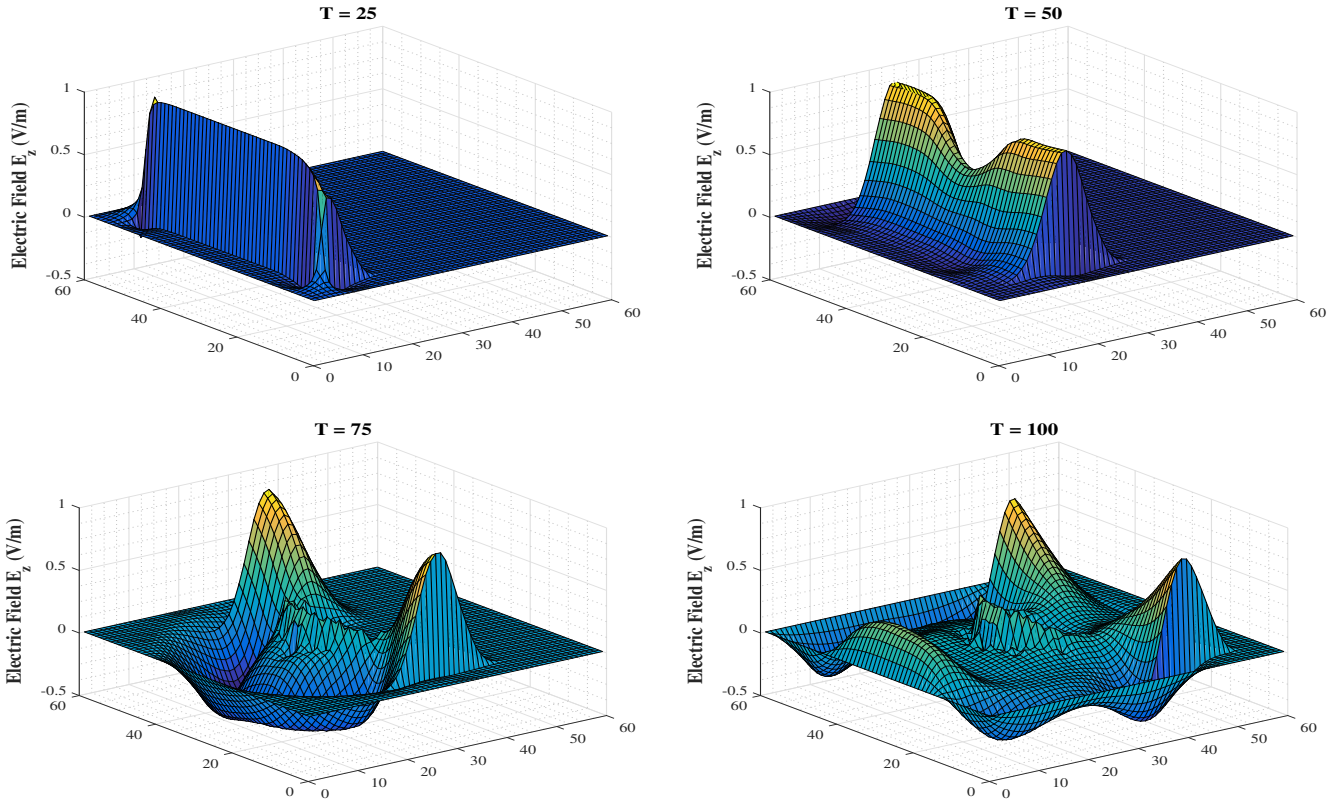

Fig. 10: Simulation of a plane wave impinging on a dielectric cylinder. The cylinder is 20 cm in diameter and has a relative dielectric constant of 30 and a conductivity of 0.3 S/m.

$$\frac{\partial \boldsymbol{H}}{\partial t} = -\frac{1}{\sqrt{\epsilon_0 \mu_0}} \nabla \times \widetilde{\boldsymbol{E}} \tag{48}$$

After expanding the above equations, we have:

$$\frac{\partial D_x}{\partial t} = \frac{1}{\sqrt{\epsilon_0 \mu_0}} \left(\frac{\partial H_z}{\partial y} - \frac{\partial H_y}{\partial z} \right) \tag{49}$$

$$\frac{\partial D_y}{\partial t} = \frac{1}{\sqrt{\epsilon_0 \mu_0}} \left(\frac{\partial H_x}{\partial z} - \frac{\partial H_z}{\partial x} \right) \tag{50}$$

$$\frac{\partial D_z}{\partial t} = \frac{1}{\sqrt{\epsilon_0 \mu_0}} \left(\frac{\partial H_y}{\partial x} - \frac{\partial H_x}{\partial y} \right) \tag{51}$$

$$\frac{\partial H_x}{\partial t} = \frac{1}{\sqrt{\epsilon_0 \mu_0}} \left(\frac{\partial E_y}{\partial z} - \frac{\partial E_z}{\partial y} \right) \tag{52}$$

$$\frac{\partial H_y}{\partial t} = \frac{1}{\sqrt{\epsilon_0 \mu_0}} \left(\frac{\partial E_z}{\partial x} - \frac{\partial E_x}{\partial z} \right) \tag{53}$$

$$\frac{\partial H_z}{\partial t} = \frac{1}{\sqrt{\epsilon_0 \mu_0}} \left(\frac{\partial E_x}{\partial y} - \frac{\partial E_y}{\partial x} \right) \tag{54}$$

After taking the finite-difference approximations on the equations (51) and (54), we have:

$$\begin{aligned} D_z^{n+1/2}\left(i,j,k+\frac{1}{2}\right) &= D_z^{n+1/2}\left(i,j,k+\frac{1}{2}\right) + \frac{\Delta t}{\Delta x \sqrt{\epsilon_0 \mu_0}} \\ &\times \left[H_y^n\left(i+\frac{1}{2},j,k+\frac{1}{2}\right) - H_y^n\left(i-\frac{1}{2},j,k+\frac{1}{2}\right) \right. \\ &\left. -H_x^{n+1}\left(i+\frac{1}{2},j+\frac{1}{2},k\right) + H_x^{n+1}\left(i+\frac{1}{2},j-\frac{1}{2},k\right) \right] \end{aligned} \tag{55}$$

$$\begin{aligned} H_z^n\left(i+\frac{1}{2},j+\frac{1}{2},k\right) &= H_z^n\left(i+\frac{1}{2},j+\frac{1}{2},k\right) + \frac{\Delta t}{\Delta x \sqrt{\epsilon_0 \mu_0}} \\ &\times \left[E_x^{n+1/2}\left(i+\frac{1}{2},j+1,k\right) - E_x^{n+1/2}\left(i+\frac{1}{2},j,k\right) \right. \\ &\left. -E_y^{n+1/2}\left(i+1,j+\frac{1}{2},k\right) + E_y^{n+1/2}\left(i,j+\frac{1}{2},k\right) \right] \end{aligned} \tag{56}$$

Fig. 11 shows the propagation of the E_z from the dipole in the XY plane level with the gap of the dipole. Of course, there is radiation in the Z direction as well. This illustrates a major problem in three-dimensional simulations: unless one has unusually good graphics, visualizing three dimensions can be difficult.

B. A Plane Wave Impinging on a Dielectric Sphere in Free Space Medium Bounded by PML

The Maxwell's equations in this case can be updated as follows:

$$\begin{aligned} \nabla \times \mathbf{H} &= H_y^n\left(i+\frac{1}{2},j,k+\frac{1}{2}\right) - H_y^n\left(i-\frac{1}{2},j,k+\frac{1}{2}\right) \\ &-H_x^{n+1}\left(i+\frac{1}{2},j+\frac{1}{2},k\right) + H_x^{n+1}\left(i+\frac{1}{2},j-\frac{1}{2},k\right) \end{aligned} \tag{57}$$

The incident electric field density is given by:

$$I_{D_z}^n\left(i,j,k+\frac{1}{2}\right) = I_{D_z}^{n-1}\left(i,j,k+\frac{1}{2}\right) + \nabla \times \mathbf{H} \tag{58}$$

$$\begin{aligned} D_z^{n+1/2}\left(i,j,k+\frac{1}{2}\right) &= gi3(i)gj3(j)D_z^{n+1/2}\left(i,j,k+\frac{1}{2}\right) \\ &+0.5gi2(i)gj2(j)\left[\nabla \times \mathbf{H} + gk1(k)I_{D_z}^{n+1/2}\left(i,j,k+\frac{1}{2}\right)\right] \end{aligned} \tag{59}$$

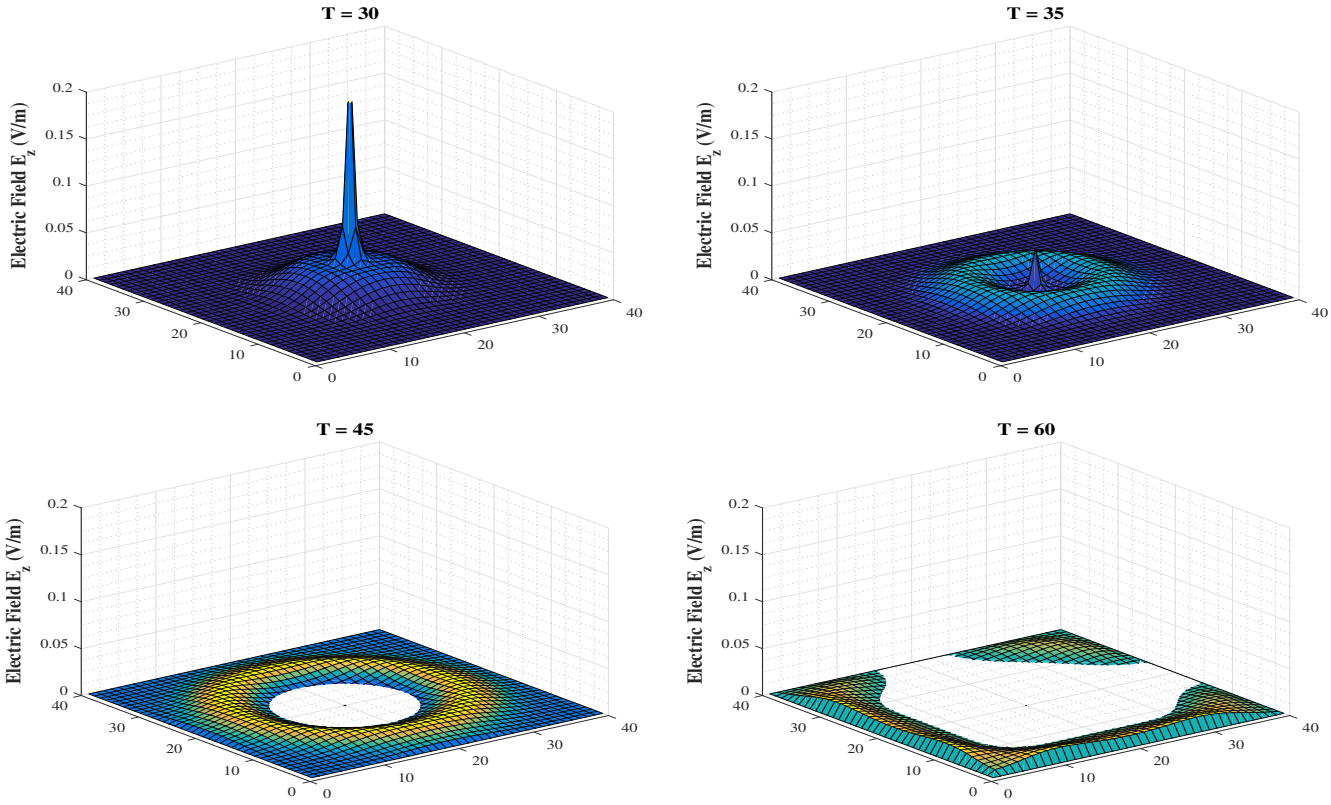

Fig. 11: E_z field radiation from a dipole antenna in a three-dimensional FDTD program.

Now that we have a program that generates a plane wave in three dimensions, we will want to start putting objects in the problem space to see how the plane wave interacts with them. In two dimensions, we chose a cylinder because we had an analytic solution with which we could check the accuracy of our calculation via a Bessel function expansion. It turns out that the interaction of a plane wave with a dielectric sphere can be determined by an expansion of the modified Bessel functions.

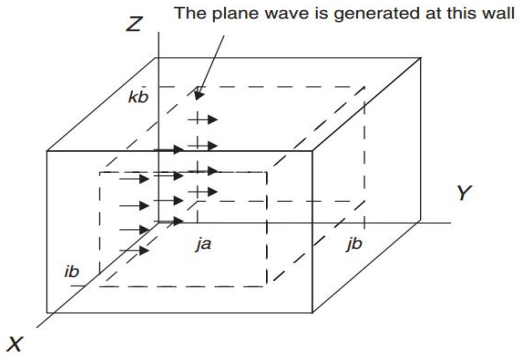

Fig. 12: Total/scattered fields in three dimensions.

The total scattered electric field density in Y direction can be obtained at the two ends by:

$$D_y\left(i, j+\frac{1}{2}, k_a\right) = D_y\left(i, j+\frac{1}{2}, k_a\right) - 0.5H_{x,inc}(j) \quad (60)$$

$$D_y\left(i, j+\frac{1}{2}, k_b+1\right) = D_y\left(i, j+\frac{1}{2}, k_b+1\right) - 0.5H_{x,inc}(j) \quad (61)$$

The analytic solutions are the same as the case of FDTD-2D.

VI. Conclusion

In this paper, we present a global framework analysis of FDTD 1D, 2D and 3D considering various combination of the medium properties such as absorbing boundaries, perfect matched layer, dielectric cylinder, etc. We provide pictorial presentations of the wave propagation in various instant to confirm the behavior of the wave in the medium with the analytic solution. In addition, we present the design of the patch antenna and the optimal parameters that provide the required antenna properties. Capitalizing on these parameters, we derive the antenna figure of merits such as the pattern, the directivity at both azimuthal and elevation planes, the input impedance, the VSWR, the return loss and the $|S_{11}|$. As an extension of this work, we intend to design an array antenna with powerful bandwidth around 60 GHz to introduce it the world of the mmWave communication. In addition, to increase the spectral efficiency, we should consider a massive MIMO that consists of latge number of small antenna (large densified array) and the design of such structure is very challenging which will be the topic of our next research work.

References

[1] E. Balti and M. Guizani, "Mixed rf/fso cooperative relaying systems with co-channel interference," *IEEE Transactions on Communications*, vol. 66, no. 9, pp. 4014–4027, 2018.

[2] E. Balti and B. K. Johnson, "Tractable approach to mmwaves cellular analysis with fso backhauling under feedback delay and hardware limitations," *IEEE Transactions on Wireless Communications*, vol. 19, no. 1, pp. 410–422, 2020.

[3] E. Balti, M. Guizani, B. Hamdaoui, and B. Khalfi, "Mixed rf/fso relaying systems with hardware impairments," in *GLOBECOM 2017 - 2017 IEEE Global Communications Conference*, 2017, pp. 1–6.

[4] E. Balti, "Analysis of hybrid free space optics and radio frequency cooperative relaying systems," Master's thesis, 2018.

[5] E. Balti, M. Guizani, B. Hamdaoui, and B. Khalfi, "Aggregate hardware impairments over mixed rf/fso relaying systems with outdated csi," *IEEE Transactions on Communications*, vol. 66, no. 3, pp. 1110–1123, 2018.

[6] E. Balti and B. K. Johnson, "On the joint effects of hpa nonlinearities and iq imbalance on mixed rf/fso cooperative systems," 2020.

[7] E. Balti, M. Guizani, and B. Hamdaoui, "Hybrid rayleigh and double-weibull over impaired rf/fso system with outdated csi," in *2017 IEEE International Conference on Communications (ICC)*, 2017, pp. 1–6.

[8] E. Balti and B. K. Johnson, "Stochastic geometry analysis of uplink cellular networks with fso backhauling: Cooperative relaying vs. reflecting surfaces," 2020.

[9] E. Balti, "Adaptive gradient search beamforming for full-duplex mmwave MIMO systems," 2020.

[10] E. Balti, N. Mensi, and D. B. Rawat, "Temporal csi correlation in mixed rf/fso cooperative relaying systems under joint effects of hpa nonlinearities and iq imbalance," 2021.

[11] E. Balti and B. L. Evans, "Adaptive self-interference cancellation for full-duplex wireless communication systems," 2021.

[12] N. Mensi, D. B. Rawat, and E. Balti, "Securing v2i communications in 5g and beyond wireless system using gradient ascent approach," 2021.

[13] Y. Maalej and E. Balti, "Cuda-accelerated application scheduling in vehicular clouds under advanced multichannel operations in wave," 2020.

[14] N. Mensi, D. B. Rawat, and E. Balti, "Pls for v2i communications using friendly jammer and double kappa-mu shadowed fading," 2020.

[15] Y. Maalej, A. Abderrahim, M. Guizani, B. Hamdaoui, and E. Balti, "Advanced activity-aware multi-channel operations1609.4 in vanets for vehicular clouds," in *2016 IEEE Global Communications Conference (GLOBECOM)*, 2016, pp. 1–6.

[16] N. Mensi, D. B. Rawat, and E. Balti, "Physical layer security for v2i communications: Reflecting surfaces vs. relaying," 2020.

[17] E. Balti and B. K. Johnson, "Rate and power adaptation for multihop regenerative relaying systems," 2021.

[18] E. Balti, "Hybrid precoding for mmwave v2x doubly-selective multiuser mimo systems," 2021.

[19] E. Balti, M. Guizani, B. Hamdaoui, and Y. Maalej, "Partial relay selection for hybrid rf/fso systems with hardware impairments," in *2016 IEEE Global Communications Conference (GLOBECOM)*, 2016, pp. 1–6.

[20] E. Balti and B. K. Johnson, "Asymmetric rf/fso relaying with hpa nonlinearities and feedback delay constraints," 2019.

[21] E. Balti and N. Mensi, "Zero-forcing max-power beamforming for hybrid mmwave full-duplex mimo systems," in *Proc. Int. Conf. on Adv. Systems and Emergent Tech.*, 2020, pp. 344–349.

[22] E. Balti and B. K. Johnson, "Sub-6 ghz microstrip antenna: Design and radiation modeling," 2019.

[23] E. Balti and M. Guizani, "Impact of non-linear high-power amplifiers on cooperative relaying systems," *IEEE Transactions on Communications*, vol. 65, no. 10, pp. 4163–4175, 2017.

[24] E. Balti and B. K. Johnson, "Mmwaves cellular v2x for cooperative diversity relay fast fading channels," 2020.

[25] N. Mensi, D. B. Rawat, and E. Balti, "Gradient ascent algorithm for enhancing secrecy rate in wireless communications for smart grid," *IEEE Transactions on Green Communications and Networking*, pp. 1–1, 2021.